ACS MATERIALS LETTERS

www.acsmaterialsletters.org

Stacking Sequence, Interlayer Bonding, Termination Group Stability and Li/Na/Mg Diffusion in MXenes

Jacob Hadler-Jacobsen, Frode Håskjold Fagerli, Henning Kaland, and Sondre Kvalvåg Schnell*

Cite This: *ACS Materials Lett.* 2021, 3, 1369–1376

Read Online

ACCESS | Metrics & More | Article Recommendations | Supporting Information

ABSTRACT: A versatile group of 2D carbide materials from the past decade, MXenes, have attracted attention for their rich chemistry and wide range of properties. The perhaps best known MXene, namely, $Ti_3C_2T_x$, has been observed to stack in two distinct ways, and simulations show that this influences interlayer bonding energy and Li diffusion. In this DFT study, six types of $Ti_3C_2T_2$ interlayer bonds resulting from O, F, and OH termination groups are assessed with respect to stability. It is shown that OH termination groups are highly stable up to 50% coverage, but unstable for higher coverage. A model to predict stacking type based on termination group chemistry shows that the degree of hydrogen bonding is the deciding factor. The model is also tested on V_2CT_2 and $Zr_3C_2T_2$, giving similar results to those of $Ti_3C_2T_2$. By calculating migration barriers for $Ti_3C_2O_2$, we show that Li, Na, and Mg have orders of magnitude faster diffusion in the stacking favored by hydrogen bonds. XRD patterns calculated for both stackings show they are close to indistinguishable, highlighting the need for caution when classifying stacking.

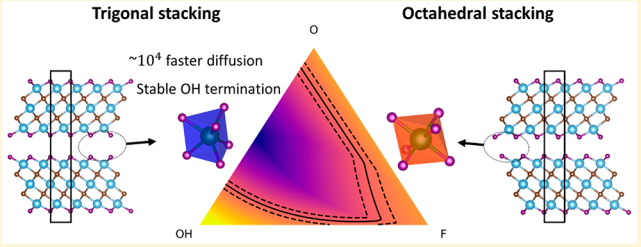

There has been much research on MXenes and their wide range of applications, such as for catalysis,[1] sensor technology,[2] optoelectronics,[3] and use in Li, Na, and Mg batteries.[4−6] However, a better understanding of the interlayer bonding and the way the 2D MXene layers stack is needed to fully utilize this group of materials. From STEM images, it can be seen that $Ti_3C_2T_x$ (T = termination, which is F, O, or OH in this work) MXenes can stack in at least two distinct ways,[4,5,7,8] which are shown in Figure 1. The first one, here described as *trigonal stacking*, consists of an AB stacking of the layers, where the termination groups are arranged facing each other, forming triangular prisms, and ions that intercalate will have trigonal prismatic coordination. This stacking has been found for HF etched $Ti_3C_2T_x$, both with and without intercalated Na ions.[5] Looking at the structure of MAX phase Ti_3AlC_2,[9] it can be seen that the trigonal stacking corresponds to the stacking obtained if the Ti_3C_2 layers in MAX phase Ti_3AlC_2 do not move during synthesis of $Ti_3C_2T_x$. The other observed stacking has every other layer moved 1/3 of a unit cell in the 110 direction relative to trigonal stacking. This stacking is also AB-type and named *octahedral stacking* in this work, as the terminations now form octahedrons, and intercalated ions would have octahedral coordination. Interestingly, this stacking has been seen in STEM images for $Ti_3C_2T_x$,[4] for Al-intercalated $Ti_3C_2T_x$,[5] and for the chloride terminated MXene $Ti_3C_2Cl_x$.[7] There are also STEM images of $Ti_3C_2T_x$ where it is unclear if there is any regular stacking,[10,11] and it has been suggested from neutron diffraction data that $Ti_3C_2T_x$ may have a mixed stacking in at least some cases.[12]

The stacking was studied with DFT in the works of Xie et al.,[13] Hu et al.,[14,15] and Thygesen et al.[16] While Thygesen et al.[16] primarily investigated how well different *van der Waals* functionals described the Ti_2CO_2 MXene, they also showed that stacking influences the migration barrier of Li in Ti_2CO_2 and found that a trigonal stacking gave orders of magnitude faster migration than an octahedral stacking. Xie et al.[13] and Hu et al.[14] found that the interlayer distance has a weak dependence on stacking but neither considered MXenes with mixed terminations. Hu et al.[15] went further in their next work and showed that interlayer hydrogen bonds favored trigonal stacking, and that other types of bonds favored octahedral stacking. Though, to the best of our knowledge, there are no previous studies considering the stability of OH termination

Received: May 28, 2021
Accepted: August 9, 2021
Published: August 16, 2021

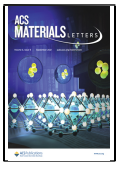

https://doi.org/10.1021/acsmaterialslett.1c00316
ACS Materials Lett. 2021, 3, 1369–1376

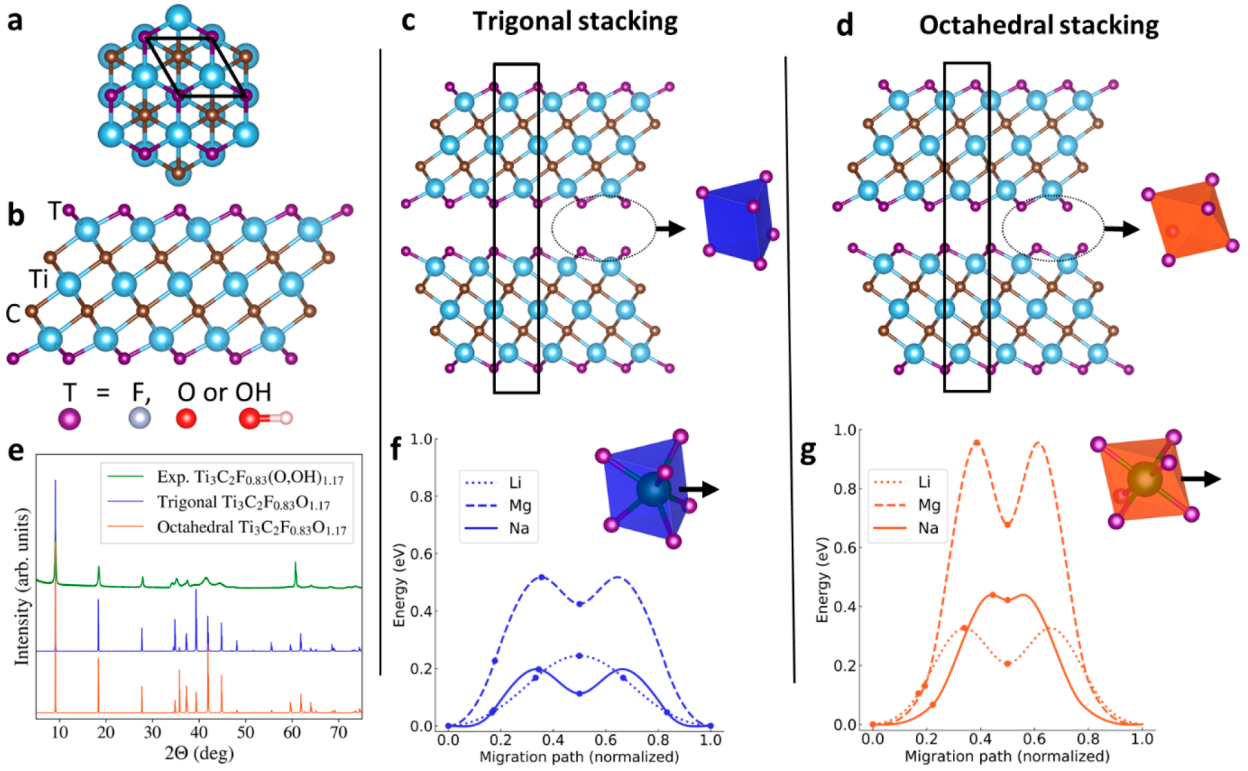

Figure 1. (a) $Ti_3C_2T_2$ seen along the *c* axis. (b) $Ti_3C_2T_2$ seen along the *a* axis, with C, Ti, and the terminations T indicated. (c and d) Two layers of $Ti_3C_2T_2$ with trigonal and octahedral type stacking, respectively. The unit cell is drawn to illustrate the AB order of both stackings. A triangular prism and an octahedron are included to show how the terminations form these geometrical shapes. (e) Calculated XRD data for $Ti_3C_2F_{0.83}O_{1.17}$ with octahedral and trigonal stacking, and experimentally obtained XRD patterns for $Ti_3C_2F_{0.83}O_{1.17}$ etched with 10% HF solution from Ti_3AlC_2 powder. The (002) reflection at $2\Theta = 9.17$ corresponds to an interlayer distance of 9.65 Å. (f and g) The (dilute limit) migration barriers for Li, Na, and Mg movement in trigonally and octahedrally stacked $Ti_3C_2O_2$ MXene. Inserts show how the Li/Mg/Na ion is coordinated in a trigonal prismatic and octahedral way.

for stacked MXenes and the interlayer bond energy and relative stability of the different stackings for mixed terminations. In this work, these properties are investigated with special emphasis on $Ti_3C_2T_2$. It is found that up to 50% of OH termination groups should be stable, and that Li, Na, and Mg migration barriers decrease several orders of magnitude between different stacking orders. Last, a model is presented, showing what stacking is most stable as a function of the termination group composition for $Ti_3C_2T_2$, V_2CT_2, and $Zr_3C_2T_2$.

Migration Barriers. To investigate the influence stacking has on diffusion, DFT calculations were performed to find migration barriers for both trigonally and octahedrally stacked $Ti_3C_2O_2$ with Li, Na, and Mg ions intercalated. The results are shown in Figure 1f and g, and the simulation setup is shown in Figure S9. Li, Na, and Mg have migration barriers of 240, 200, and 520 meV for the trigonal stacking, respectively, confirming that the divalent Mg will exhibit a much more sluggish diffusion. For octahedral stacking, the trend is the same, but with significantly higher barriers for all species, at 330, 440, and 960 meV, respectively, for Li, Na, and Mg. It is possible to estimate the relative diffusivity of Li, Na, and Mg by assuming that the diffusion coefficient is proportional to $\exp(E_B/k_BT)$, where E_B is the migration barrier, k_B is the Boltzmann constant, and T is the absolute temperature. This shows that trigonal stacking performs much better than octahedral stacking with 30 times faster Li diffusion, $\sim 10^4$ times faster Na diffusion, and impressively $\sim 10^7$ times faster Mg diffusion. In other words, ensuring trigonal stacking may be critical if the $Ti_3C_2T_2$ MXene is to be used in electrochemical storage applications based on intercalation, especially for Na and even more so for Mg. The migration barriers also show that Mg diffusion is 4 to 10 orders of magnitude slower than Li and Na diffusion for trigonal and octahedral stacking. This may help explain why it has been proven difficult to intercalate unsolvated Mg ions in MXenes.[6]

Experimental and Theoretical XRD Patterns. An important and more practical question when considering the importance of stacking for intercalation is whether the trigonal and octahedral stacking can be distinguished by XRD. To test this, theoretical XRD patterns were calculated for both stackings and compared to an experimentally obtained XRD pattern for a MXene with the composition measured to $Ti_3C_2F_{0.83}(O,OH)_{1.17}$ by EDS (assuming $Ti_3C_2T_x$ with $x = 2$). The XRD patterns are shown in Figure 1e, Figure S1, and Figure S2. The calculated trigonal and octahedral patterns closely resemble each other, where the major difference relates to a relative intensity difference between the peaks, especially for the ones at $2\theta = 35.8$ and $2\theta = 39.4$. Seeing that there is no perfect match between the experimental XRD pattern and any of the two theoretical patterns, it is not possible to determine the stacking of the as-synthesized MXene. This agrees well with a previous report where the calculated XRD patterns for trigonally and octahedrally stacked $Ti_3C_2O_2$ were found to be too similar to determine the dominant stacking.[14] The challenge is further magnified given the possibility of both mixed stacking and mixed termination groups. Figure S2 demonstrates how the different termination groups adjust the

https://doi.org/10.1021/acsmaterialslett.1c00316
ACS Materials Lett. 2021, 3, 1369−1376

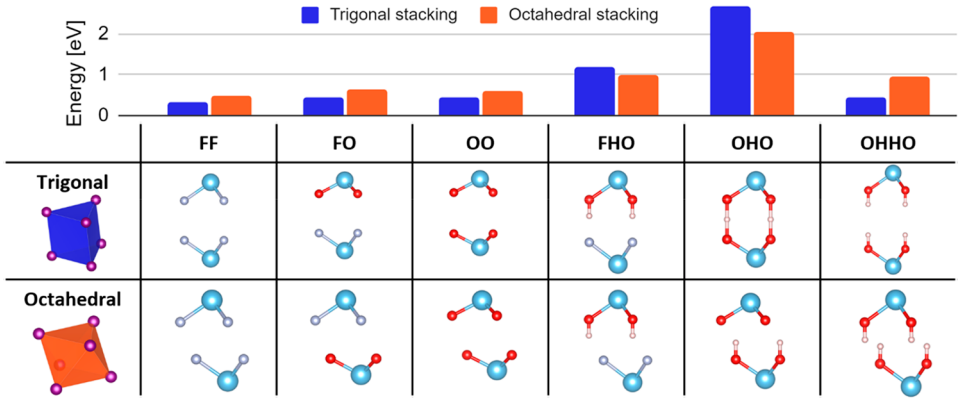

Figure 2. Different bond types for trigonal and octahedral stacking and their interlayer bond energy. The energy is shown for one bond, and there is one bond for each formula unit of $Ti_3C_2T_2$.

Table 1. Proposed Reactions Involving the Interlayer Bonds, Their Calculated Reaction Energies, and Their Equilibrium Constants, *K*[a]

		trigonal stacking		octahedral stacking	
	reactions	reaction energy [eV]	*K*	reaction energy [eV]	*K*
1	$OHHO \rightarrow OHO + 1/2H_2$	−0.97	2.5×10^{16}	−0.39	3.2×10^{6}
2	$OO + 1/2H_2 \rightarrow OHO$	−1.12	8.0×10^{18}	−0.71	9.0×10^{11}
3	$FO + 1/2H_2 \rightarrow FHO$	−0.52	6.3×10^{8}	−0.34	4.8×10^{5}
4	$OO + FHO \rightarrow OHO + FO$	−0.60	1.3×10^{10}	−0.37	1.9×10^{6}
5	$OHHO + FO \rightarrow OHO + FHO$	−1.49	1.6×10^{25}	−0.72	1.5×10^{12}
6	$OHHO + OO \rightarrow 2OHO$	−2.09	2.0×10^{35}	−1.09	2.9×10^{18}

[a]Corresponding reaction energies for V_2CT_2 and $Zr_3C_2T_2$ can be found in Table S1.

peak locations, in addition to altering the relative peak intensities of some peaks. This peak shift may again explain the broad XRD peaks observed experimentally, seeing that a potential nonrandom distribution of the termination groups would lead to broadening of the XRD peaks. With these challenges in mind, it is questionable if XRD alone is suited to determine the stacking of as-synthesized MXenes. However, accompanied by extensive STEM imaging, XRD may still prove a possible tool to give information about the bulk stacking of MXenes. Also worth mentioning is that Wang et al.[12] used the fitting of an atomic pair distribution function obtained from neutron diffraction data to study the structural properties of $Ti_3C_2O_2$ and showed that the stacking appeared to go from octahedral to a mix of octahedral and trigonal when the synthesis conditions were changed. Investigations of the stacking order are possible, although they require more extensive techniques than normal XRD.

Interlayer Bonding. The three different terminations thought to make up the T group in HF-etched $Ti_3C_2T_2$ MXene, namely, F, O, and OH, can result in six interlayer bonds if only pair interactions between facing terminations are considered. These six bonds are shown in Figure 2 with their accompanying bond energy for $Ti_3C_2T_2$. Interlayer distances for $Ti_3C_2T_2$ can be found in Figure S3 and bond energies for $Ti_3C_2T_2$, V_2CT_2, and $Zr_3C_2T_2$ in Figure S4. The bonds involving only O and F atoms are of van der Waals character, with a clear trend that octahedral stacking has higher bond strength compared to trigonal stacking. The FHO and OHO bonds on the other hand display strong hydrogen bonding, with trigonal stacking having a much higher bond strength than the octahedral stacking. Only FHO- and OHO-bond types favor trigonal stacking energetically, and therefore it seems natural to assume that $Ti_3C_2T_2$ experimentally found to have trigonal stacking must have more FHO and OHO bonds than the octahedrally stacked MXenes.

OHHO stands out from the other bond types, with the trigonal stacking and OHHO giving rise to a very large interlayer distance of 11.3 Å (Figure S3). This value is considerably larger than the other bonds described here and the typical interlayer distances around ∼9.4−10 Å found experimentally for untreated HF etched $Ti_3C_2T_2$ with mixed termination.[17] Thus, it is only for $Ti_3C_2T_2$ made with other synthesis routes and with larger interlayer spacing that it seems possible with OHHO bonds for the trigonal stacking, considering interlayer distances alone.

Reactions Involving Interlayer Bonds. To investigate the stability of the different bond types in $Ti_3C_2T_2$, the energies of proposed reactions for the bonds in Figure 2 were calculated and are presented in Table 1. The reaction energies and corresponding equilibrium constants show that the stability of the OHHO bond is very low for MXenes with trigonal stacking, but also low for octahedrally stacked MXenes. A consequence of this instability is that there is a large driving force for OHHO bonds giving hydrogen to FO and especially OO type bonds if possible, as evident from the equilibrium constants for reactions 5 and 6 in Table 1. This further suggests that OHHO bonds for stacked MXenes with interlayer distances below 10 Å are unlikely for both stackings and would only exist in a metastable state. Especially if heat treatment is applied postsynthesis to increase the chance that equilibrium is reached, it is hard to imagine more than 50% OH termination, as that would imply the existence of OHHO bonds.

To see if this applies to other MXenes than $Ti_3C_2T_2$, the same calculations were performed for V_2CT_2 and $Zr_3C_2T_2$. The results are given in Table S1 and show a trend with highly

https://doi.org/10.1021/acsmaterialslett.1c00316
ACS Materials Lett. 2021, 3, 1369−1376

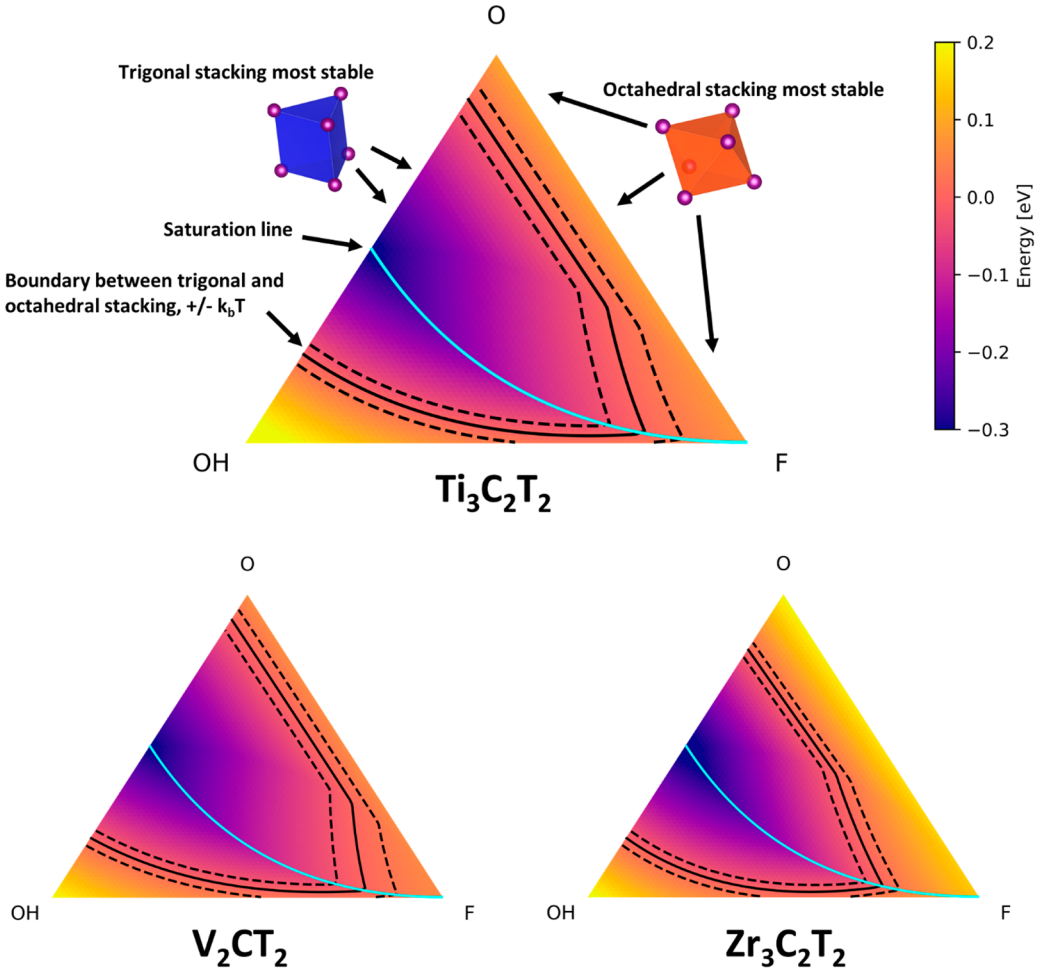

Figure 3. Reaction energy for going from octahedral stacking to trigonal stacking as predicted by the model, for $Ti_3C_2T_2$, V_2CT_2, and $Zr_3C_2T_2$. Negative energy implies that trigonal stacking is most stable. The solid and dotted contour lines show where the reaction energy is zero and $\pm k_BT$, respectively, and the area between the dotted lines represents termination group combinations where a mixture of the two stackings is expected. The cyan line indicates compositions where all OO and FO bonds have absorbed H_2 and become OHO and FHO; i.e., the MXene is saturated with H_2. The area to the left of the cyan line is where there are OHHO bonds present, which would decompose to OHO according to the model. The termination group compositions within this area are therefore unstable.

unstable OHHO bonds for all three MXenes. There are a few differences, however, with $Zr_3C_2T_2$ appearing to have a somewhat weaker driving force for reactions 2 and 3, with the octahedrally stacked $Zr_3C_2T_2$ even having a positive reaction energy. From Figure S4, this appears to be due to $Zr_3C_2T_2$ having both a weaker FHO bond and a stronger FO and OO bond. The bonding in V_2CT_2 on the other hand seems to have no particular features distinguishing it from $Ti_3C_2T_2$.

The OO and FO bonds' affinity for adsorbing H and the fact that hydrogen gas evolves during the synthesis of MXenes[18] suggest that pure FO and OO bonding may be rare if there are no significant kinetic barriers present during synthesis. Especially if the MXene has been post treated with H_2 at elevated temperatures, as was done by Cheng et al.[4] They saw a slight change in the XRD pattern and a shift in the cycling performance, but they did not investigate changes in interlayer bonds or stacking. It is therefore hard to tell if the changes were due to changes in stacking and/or bonding.

If the $Ti_3C_2T_2$ MXene is only terminated with O and OH terminations, the bond stabilities based on Table 1 suggest that $Ti_3C_2O(OH)$ should be more stable than $Ti_3C_2(OH)_2$ and $Ti_3C_2O_2$. This applies for both octahedral and especially trigonal stacking, and the reason is the stability of the OHO-bond being higher than that of the OHHO and OO bonds. The high stability of stacked $Ti_3C_2O(OH)$ is especially worth noticing, as it is typically the purely terminated single layer $Ti_3C_2(OH)_2$ and $Ti_3C_2O_2$ that is considered in theoretical studies.[19−21] Furthermore, the stability of OH-termination groups may be influenced by applied potentials. For instance, if an anodic (oxidizing) potential is applied to $Ti_3C_2O(OH)$, it would provide a driving force for the reaction $Ti_3C_2O(OH) \rightarrow Ti_3C_2O_2 + H^+ + e^-$. Similarly, if a cathodic (reductive) potential is applied to the MXene in contact with a proton bearing electrolyte such as water, there would be a driving force for the opposite reaction, or for further reduction. In either case, the reaction will be dependent on pH, as H^+ is involved. Thus, both pH and potential are important to keep in mind when utilizing MXenes for either anode or cathode applications. However, they may also present ways to tune the degree of OH termination between the layers and, thus, also indirectly the relative stability of the stackings, since $Ti_3C_2O(OH)$ strongly favors trigonal stacking. As to the relevance of only O and OH terminated MXenes, it is worth noting that there is an ever increasing amount of reports on synthesizing fluorine free $Ti_3C_2T_2$.[8,22,23]

https://doi.org/10.1021/acsmaterialslett.1c00316
ACS Materials Lett. 2021, 3, 1369−1376

There has been some debate as to the existence of OH termination.[24] Both theoretical[20] and experimental work[25] have suggested that OH termination is unstable or does not exist. However, the stability of FHO and OHO bonds, evident from reactions 2 and 3 in Table 1, implies OH termination indeed is stable and exists. This discrepancy may in part be because the earlier theoretical work[20] looked at single MXene layers in a vacuum and not stacked MXenes as in this work.

A Model to Predict Stacking. With data from the DFT simulations, a model to predict the energetic driving force for preferred stacking as a function of O, OH, and F termination group composition was developed. As can be seen in Figure 3, the model shows that all compositions free of OH prefer the octahedral stacking, while the trigonal stacking is at its most stable when there is an equimolar mix of O and OH termination, resulting in only OHO type bonds. Also worth noticing are the significant areas in Figure 3 where the difference between the two stackings is smaller than k_BT at room temperature, suggesting that a mixture of the two stackings may be common. This corresponds well with a recent report suggesting that mixed stackings can be present in MXenes.[12] The case of all FO and OO bonds adsorbing H is shown with a cyan line in Figure 3. If the hydrogen present during the synthesis of the MXene has not already hydrogenated the available FO and OO bonds, an as-mentioned H_2 post treatment of the MXene could be expected to drive the composition toward this line. The driving force for hydrogenation happening in the case of $Zr_3C_2T_2$ would be lower. However, the effect of this is likely not too large since reaction 3 in Tables 1 and S1 is spontaneous for trigonal stacking, and since trigonal stacking would to a high degree be favored after OHO bonds are made through the spontaneous reaction 2. To the left of the cyan colored line is an area where there are so many OH terminations that OHHO bonds must exist, based on this model. However, considering the high driving force for OHHO to decompose to OHO as mentioned previously, it seems likely that this area would be thermodynamically unstable, and thus limit how much OH there can be in stacked HF-etched MXene. In addition, Figure 3 also demonstrates how a minimum of ∼11%, 8%, and 18% OH termination is required for the trigonal stacking to be thermodynamically stable for $Ti_3C_2T_2$, V_2CT_2, and $Zr_3C_2T_2$, respectively. This again strengthens the argument for the existence of OH terminations, seeing that the trigonal stacking already has been observed experimentally.

We hope the results presented in this work can inspire further studies of MXene stacking. For instance, measurements of termination group chemistry combined with measurements of the stacking through STEM or neutron diffraction could provide useful insight into the interlayer chemistry of the MXenes. Though, STEM imaging would require many images to avoid small sample bias, and interpreting stacking from neutron scattering data is likely to need the employment of a model.[12] However, the different stackings may still be possible to study indirectly through how they affect diffusivity, especially if only small amounts of Li/Na/Mg are intercalated. Another finding in this work which is worth investigating is that OH-termination groups should be stable, especially for compositions such as $Ti_3C_2O(OH)$ and other compositions at or to the right of the cyan lines in Figure 3. This would again affect how MXenes respond to heat treatment, hydrogenation, and maybe also applied potentials and pH. However, it is important to bear in mind that these results apply for stacked MXenes, and not necessarily to MXenes with larger interlayer distances, such as delaminated MXenes.

Two different stackings seen in STEM images of $Ti_3C_2T_2$ MXene were investigated with DFT: trigonal and octahedral. It has been shown that it is difficult to tell the subtle structural difference between the stackings by XRD. Yet, this subtle structural difference gives rise to several orders of magnitude faster diffusion for trigonal stacking compared to octahedral stacking for Li, Na, and Mg ions in $Ti_3C_2O_2$. The trigonal stacking is preferred by OHO and FHO bonds, while FF, FO and OO bonds prefer octahedral stacking. The OHHO bond was shown to be unstable with respect to decomposition to H_2 and OHO for both stackings and for all MXenes investigated, namely, $Ti_3C_2O_2$, V_2CT_2, and $Zr_3C_2T_2$. The FHO and especially OHO bonds proved to be very stable on the other hand, and since OH termination is a prerequisite for OHO and FHO bonding, this strongly suggests that the disputed OH termination should also be stable under such conditions. A model was made based on bond energies, to show how the preferred stacking varies with O, F, and OH composition of the termination groups. This model indicates that at least ∼11% OH termination is needed to obtain trigonal stacking for $Ti_3C_2O_2$ and that there are compositions where the stackings are close in energy so that a mixture of both stackings may be expected. Regarding the differences between the three investigated MXenes, $Zr_3C_2T_2$ stood out to a small degree with a slightly less stable FHO bond and a stronger preference for octahedral stacking. Nevertheless, the main trends seemed to apply for all three MXenes, and especially $Ti_3C_2T_2$ and V_2CT_2 showed very similar behavior. All in all, this work has showed that intercalation kinetics for Li/Na/Mg, termination group chemistry, and stacking are all strongly dependent on one another. Hopefully, this will inspire investigations combining electrochemical cycling, termination group measurements, and STEM imaging to cast further light on MXene properties and how stacking and termination groups can be tuned to control these properties.

METHODS

Computational. All calculations were performed with the plane wave DFT code *Vienna Ab Initio Simulation package* (VASP),[26−28] version 5.4.4, with the functional being GGA-type PBEsol[29] described by the projector augmented wave method (PAW).[30] The cutoff for the plane waves was 450 eV. The pseudopotentials were chosen among those supplied with VASP and were the C, O, F, Li, Na_pv, Mg_pv, Ti_pv, V_sv, and Zr_sv potentials with 4, 6, 7, 1, 7, 8, 10, 13, and 12 valence electrons, respectively. On the basis of Thygesen et al.'s test of vdW functionals for MXenes,[16] D3-type vdW corrections were used.[31] All calculations were performed at 0 K. For geometrical relaxation, the conjugate gradient method was used to get all forces below 0.01 eV $Å^{-1}$. 12 × 12 × 2 k points were used when calculating on unit cells, as shown in Figure S7 and Figure 1a, c, and d, giving the results used in Figures 2, 3, S3, and S4 and Tables 1 and S1. 4 × 4 × 1 k points were used for calculating the migration barriers, which were calculated for a 3 × 3 × 1 supercell (stoichiometry Li/Na/Mg $Ti_{54}C_{36}O_{36}$), with a >20 Å vacuum between the layers, as shown in Figure S9. All k points were generated with the Monkhorst Pack method. The energy of H_2, used for finding reaction energies in Table 1 and Table S1, was calculated for a H_2 molecule in a 30 × 30 × 30 Å simulation cell. All reaction energies in Table 1 and Table S1 were calculated simply by adding and subtracting the 0 K

https://doi.org/10.1021/acsmaterialslett.1c00316
ACS Materials Lett. 2021, 3, 1369−1376

energies obtained for trigonally and octahedrally stacked Mxene in addition to the H_2 molecule. This assumes that the effect of neglecting entropy and assuming the difference in heat capacities of reactants and products to be small compared to the resulting energies. The equilibrium constants K were calculated from $K = \exp(-E/k_BT)$, where E is the reaction energy, k_B is the Boltzmann constant, and T is the absolute temperature in Kelvin. The interlayer bond energy was calculated as the energy difference between stacked MXene layers and MXene layers separated with a >20 Å vacuum, as shown in Figure S8. The interlayer distance is obtained by dividing the c-lattice parameter for stacked MXene, Figure S8a), by 2. Vesta was used for visualization of atomic structures.[32]

The *Climbing Image Nudged Elastic Band* method (cNEB)[33] was used for finding the migration barriers for purely oxygen terminated $Ti_3C_2T_2$ MXene, i.e., $Ti_3C_2O_2$. The forces were relaxed to <0.01 eV $Å^{-1}$, using both the *Fast Inertial Relaxation Engine* (FIRE) method and the conjugate gradient method. One end point was placed in the most stable site, which is where the octahedron and triangular prism are drawn in Figure 1 and which is also shown as solid circles in Figure S9. The second end point is metastable and on a neighboring site, shown as dashed circles in Figure S9. For trigonal stacking, this end point would have trigonal prismatic coordination with the termination groups and reside between two titanium atoms, while for the octahedral stacking it is inside a tetrahedron, with the Li/Na/Mg placed between a termination group and a titanium atom as seen in Figure S9. Figure 1f and g show the NEB images and start/end points as dots, and a spline fit to the data made with the Henkelmann groups code is drawn as lines, mirrored around the metastable point halfway ($x = 0.5$) along the migration path in Figure 1f and g. For all cNEB calculations, two images were employed between the most stable and the metastable site, except for Li in trigonal stacked $Ti_3C_2O_2$, which employed five images between the two most stable sites. The transition state at $x = 0.5$ for Li in trigonal stacking appeared identical to that of the metastable site of Na and Mg.

The calculated XRD patterns in Figure 1e were obtained by relaxing three 3 × 3 supercells ($Ti_{54}C_{36}F_{15}O_{21}$) for each stacking, with randomly placed F and O, and plotting them on top of each other. The geometrical relaxation was performed with the interlayer distance fixed to match the experimentally obtained interlayer distance of 9.65 Å, with all other parameters free. The three patterns with random placement of F and O were nearly identical, showing that the random placement of F and O $Ti_{54}C_{36}F_{15}O_{21}$ influences the pattern to little degree. The patterns for $Ti_3C_2F_2$ and $Ti_3C_2O_2$ were also calculated and did show some slight deviations from $Ti_{54}C_{36}F_{15}O_{21}$ as seen in Figure S2.

Experimental Section. $Ti_3C_2T_x$ MXene was synthesized by etching 2.5 g of wet ball milled commercial Ti_3AlC_2 powder (Laizhou Kai Kai Ceramic Materials Co., Ltd.) in 50 mL of 10 wt. % HF for 24 h. After the etching process, the powder was washed several times by centrifugation, decantation, and refilling of DI water, until the pH reached ∼5. The composition of the termination groups was found by averaging values from 10 EDS point scans from different particles with 15 kV acceleration voltage and assuming only F and O terminations were present. This was performed in an LVFESEM Zeiss SUPRA 55VP. The XRD spectra were obtained by powder diffraction on a Bruker D8 Focus Diffractometer, with a Cu Kα radiation source (λ = 1.5406 Å), a divergence slit of 0.2 mm, and a scanning program from 5° to 75° 2θ values with a step size of 0.0143 and a dwelling time of 0.68 s.

Model for Interlayer Bonding Energy and Preferred Stacking for Mixed Termination MXenes. The input for the model is the fraction of O, F, and OH in a MXene. The output is the energy released when going from octahedral to trigonal stacking. To accomplish this, the model needs a list of the interlayer bond energies for the six bonds shown in Figure 2. In this work those energies are calculated with DFT. Since both the trigonal and octahedral bond energies are obtained relative to the same reference of a single layer in a vacuum, the vacuum reference cancels out, and the model does in fact only depend on the relative stability of the trigonal and octahedral stacking. This is advantageous, as the accuracy of DFT is best when comparing very similar (bulk) systems as in the case of these two stackings. The results of the model can be seen in Figure 3, Figure S3, and Figure S4. The main assumptions used are (1) complete termination, i.e., the stoichiometry is $Ti_3C_2T_2$; (2) F and O are distributed at random; (3) H is placed randomly, but with a total preference for OHO placement over FHO, and for FHO placement over OHHO; this preferential placement is based on the reaction energies in Table 1 and Table S1; (4) The average bond energy can be assumed equal to the linear combination of the pure FF, FO, OO, FHO, OHO, and OHHO (DFT) bond energies.

The model details are as follows. It was assumed that the MXene has a total of two termination groups per formula unit and that the termination consists of F, O, and OH. $Ti_3C_2T_2$ can then be written:

$$Ti_3C_2F_xO_yOH_{2-x-y} \tag{1}$$

The fractions of the different terminations are defined

$$X_F = \frac{x}{2},\ X_O = \frac{y}{2},\ X_{OH} = \frac{2-x-y}{2} \tag{2}$$

The goal of the model is to obtain a function E_i (X_F,X_O,X_{OH}) where E_i is the interlayer bonding energy for trigonally or octahedrally stacked $Ti_3C_2T_2$. This function can then be used to find the reaction energy for going from one stacking to the other: $E_{rx} = E_{Octahedral} - E_{Trigonal}$.

First, the fraction of terminations being in either O or OH form, θ, is defined as

$$X_\theta = X_O + X_{OH} \tag{3}$$

There is a total of six different bond types included in this model: FF, FHO, FO, OHHO, OHO, and OO. To find the amount of these bonds, it is assumed that O (both from O termination and OH termination) and F atoms are placed randomly on the Ti_3C_2. The bonds are denoted with B_n where n = FF, FHO, FO, OHHO, OHO, or OO. Since there is one bond formed for every formula unit of $Ti_3C_2T_2$, B_n corresponds to both the fraction of the bond and the number of moles per formula unit of a bond.

The following equations describe the correlation between the fractions of different terminations X and the moles of different bond types B per formula unit $Ti_3C_2F_xO_yOH_{2-x-y}$:

$$X_F^2 = B_{FF} \tag{4}$$

$$2X_\theta X_F = B_{FHO} + B_{FO} \tag{5}$$

https://doi.org/10.1021/acsmaterialslett.1c00316
ACS Materials Lett. 2021, 3, 1369−1376

$$X_\theta^2 = B_{OHHO} + B_{OHO} + B_{OO} \quad (6)$$

and the following equation describing the mass balance for hydrogen:

$$2X_{OH} = n_{OH} = 2B_{OHHO} + B_{OHO} + B_{FHO} \quad (7)$$

Instead of assuming random placement of H in the system (which would result in X_{OH}^2 = OHHO, X_O^2 = OO, $2X_OX_{OH}$ = OHO), it is assumed that hydrogen is placed in OHO and FHO type bonds before OHHO-type bonds, due to reactions 5 and 6 in Table 1 being very energetically favored. Similarly, it is assumed that the hydrogen is placed in OHO bonds before FHO bonds due to reaction 4 in Table 1 being strongly in favor of OHO. This leads to the need for solving for B_n for three separate cases depending on how much hydrogen, n_{OH}, there is in the system:

The first case is if $X_\theta^2 > 2X_{OH}$:

$$B_{OHO} = 2X_{OH} \quad (8)$$

$$B_{FHO} = 0 \quad (9)$$

$$B_{OHHO} = 0 \quad (10)$$

The second case is if $X_\theta^2 < 2X_{OH} < X_\theta^2 + 2X_\theta X_F$:

$$B_{OHO} = X_\theta^2 \quad (11)$$

$$B_{FHO} = 2X_{OH} - X_\theta^2 \quad (12)$$

$$B_{OHHO} = 0 \quad (13)$$

And the third case is if $X_\theta^2 + 2X_\theta X_F < 2X_{OH}$:

$$B_{OHO} = X_\theta^2 \quad (14)$$

$$B_{FHO} = 2X_\theta X_F \quad (15)$$

$$B_{OHHO} = 2X_{OH} - 2X_\theta X_F - X_\theta^2 \quad (16)$$

while B_{FF}, B_{FO}, and B_{OO} can be found from the following equations for all cases:

$$B_{OO} = X_\theta^2 - B_{OHHO} - B_{OHO} \quad (17)$$

$$B_{FO} = 2X_FX_\theta - B_{FHO} \quad (18)$$

$$B_{FF} = X_F^2 \quad (19)$$

All bonds are then known, and the bonding energy for the system can then be found from

$$E_i = \sum_n \epsilon_n B_n \quad (20)$$

where ϵ_n is the interlayer bonding energy per formula unit for n = FF, FHO, FO, OHHO, OHO, and OO, as displayed in Figure 2. $E_{Octahedral}$ and $E_{Trigonal}$ can be found in Figure S5, while $E_{rx} = E_{Octahedral} - E_{Trigonal}$ is plotted in Figure 3 and Figure S4. To obtain the solid blue line in Figure 3 and Figure S4, the following equation is solved:

$$2X_{OH} = X_\theta^2 + 2F\theta \quad (21)$$

giving the solution:

$$X_O = \frac{1}{2}X_F^2 - F + \frac{1}{2} \quad (22)$$

The dotted blue line in Figure S4 is obtained by solving:

$$2X_{OH} = X_\theta^2 \quad (23)$$

giving the solution:

$$X_O = -\frac{1}{2}X_F^2 + \frac{1}{2} \quad (24)$$

the magenta line is simply X_F = 0.415 plotted.

■ ASSOCIATED CONTENT

Supporting Information

The Supporting Information is available free of charge at https://pubs.acs.org/doi/10.1021/acsmaterialslett.1c00316.

Additional XRD patterns, bond energy and interlayer distance data, data related to the model and figures illustrating NEB-path, VASP input and output files (PDF)

■ AUTHOR INFORMATION

Corresponding Author

Sondre Kvalvåg Schnell − *Department of Materials Science and Engineering, Norwegian University of Science and Technology, NTNU, NO-7491 Trondheim, Norway;* orcid.org/0000-0002-0664-6756; Email: sondre.k.schnell@ntnu.no

Authors

Jacob Hadler-Jacobsen − *Department of Materials Science and Engineering, Norwegian University of Science and Technology, NTNU, NO-7491 Trondheim, Norway*

Frode Håskjold Fagerli − *Department of Materials Science and Engineering, Norwegian University of Science and Technology, NTNU, NO-7491 Trondheim, Norway;* orcid.org/0000-0001-9764-1602

Henning Kaland − *Department of Materials Science and Engineering, Norwegian University of Science and Technology, NTNU, NO-7491 Trondheim, Norway;* orcid.org/0000-0002-5886-9521

Complete contact information is available at: https://pubs.acs.org/10.1021/acsmaterialslett.1c00316

Author Contributions

J.H. and S.K.S. conceived the concept. J.H. performed the simulations, made the model, and wrote the nonexperimental parts of the paper. F.H.F. performed the experimental work and wrote the experimental part of the paper. S.K.S. supervised the research. All authors discussed the results and contributed to the writing of the manuscript.

Notes

The authors declare no competing financial interest.

■ ACKNOWLEDGMENTS

The computations were performed on resources provided by UNINETT Sigma2 - the National Infrastructure for High Performance Computing and Data Storage in Norway for project NN9414K.

■ REFERENCES

(1) Zhang, Z.; Li, H.; Zou, G.; Fernandez, C.; Liu, B.; Zhang, Q.; Hu, J.; Peng, Q. Self-Reduction Synthesis of New MXene/Ag Composites with Unexpected Electrocatalytic Activity. *ACS Sustainable Chem. Eng.* **2016**, *4*, 6763−6771.

(2) Wang, F.; Yang, C. H.; Duan, M.; Tang, Y.; Zhu, J. F. TiO2 nanoparticle modified organ-like Ti3C2MXene nanocomposite

encapsulating hemoglobin for a mediator-free biosensor with excellent performances. *Biosens. Bioelectron.* **2015**, *74*, 1022−1028.
(3) Kim, H.; Alshareef, H. N. MXetronics: MXene-Enabled Electronic and Photonic Devices. *ACS Mater. Lett.* **2020**, *2*, 55−70.
(4) Cheng, R.; Hu, T.; Zhang, H.; Wang, C.; Hu, M.; Yang, J.; Cui, C.; Guang, T.; Li, C.; Shi, C.; Hou, P.; Wang, X. Understanding the Lithium Storage Mechanism of Ti3C2Tx MXene. *J. Phys. Chem. C* **2019**, *123*, 1099−1109.
(5) Wang, X.; Shen, X.; Gao, Y.; Wang, Z.; Yu, R.; Chen, L. Atomic-scale recognition of surface structure and intercalation mechanism of Ti3C2X. *J. Am. Chem. Soc.* **2015**, *137*, 2715−2721.
(6) Kaland, H.; Hadler-Jacobsen, J.; Fagerli, F. H.; Wagner, N. P.; Wang, Z.; Selbach, S. M.; Vullum-Bruer, F.; Wiik, K.; Schnell, S. K. Are MXenes suitable as cathode materials for rechargeable Mg batteries? *Sustain. Energy Fuels* **2020**, *4*, 2956−2966.
(7) Li, M.; Lu, J.; Luo, K.; Li, Y.; Chang, K.; Chen, K.; Zhou, J.; Rosen, J.; Hultman, L.; Eklund, P.; Persson, P. O. Å.; Du, S.; Chai, Z.; Huang, Z.; Huang, Q. Element Replacement Approach by Reaction with Lewis Acidic Molten Salts to Synthesize Nanolaminated MAX Phases and MXenes. *J. Am. Chem. Soc.* **2019**, *141*, 4730−4737.
(8) Kamysbayev, V.; Filatov, A. S.; Hu, H.; Rui, X.; Lagunas, F.; Wang, D.; Klie, R. F.; Talapin, D. V. Covalent surface modifications and superconductivity of two-dimensional metal carbide MXenes. *Science* **2020**, *369*, 979−983.
(9) Zhou, Y. C.; Wang, X. H.; Sun, Z. M.; Chen, S. Q. Electronic and structural properties of the layered ternary carbide Ti3AlC2. *J. Mater. Chem.* **2001**, *11*, 2335−2339.
(10) Lu, J.; Persson, I.; Lind, H.; Palisaitis, J.; Li, M.; Li, Y.; Chen, K.; Zhou, J.; Du, S.; Chai, Z.; Huang, Z.; Hultman, L.; Eklund, P.; Rosen, J.; Huang, Q.; Persson, P. O. Å. Tin+1Cn MXenes with fully saturated and thermally stable Cl terminations. *Nanoscale Adv.* **2019**, *1*, 3680−3685.
(11) Halim, J.; Lukatskaya, M. R.; Cook, K. M.; Lu, J.; Smith, C. R.; Naslund, L.-A.; May, S. J.; Hultman, L.; Gogotsi, Y.; Eklund, P.; Barsoum, M. W. Transparent conductive two-dimensional titanium carbide epitaxial thin films. *Chem. Mater.* **2014**, *26*, 2374−2381.
(12) Wang, H. W.; Naguib, M.; Page, K.; Wesolowski, D. J.; Gogotsi, Y. Resolving the Structure of Ti3C2Tx MXenes through Multilevel Structural Modeling of the Atomic Pair Distribution Function. *Chem. Mater.* **2016**, *28*, 349−359.
(13) Xie, Y.; Naguib, M.; Mochalin, V. N.; Barsoum, M. W.; Gogotsi, Y.; Yu, X.; Nam, K.-W.; Yang, X.-Q.; Kolesnikov, A. I.; Kent, P. R. C. Role of Surface Structure on Li-ion Energy Storage Capacity of Two-dimensional Transition Metal Carbides. *J. Am. Chem. Soc.* **2014**, *136*, 6385−6394.
(14) Hu, T.; Zhang, K.; Wang, J.; Li, Z.; Hu, M.; Tan, J.; Hou, P.; Li, F.; Wang, X. Anisotropic electronic conduction in stacked two-dimensional titanium carbide. *Sci. Rep.* **2015**, *5*, 1−8.
(15) Hu, T.; Hu, M.; Li, Z.; Zhang, H.; Zhang, C.; Wang, J.; Wang, X. Interlayer coupling in two-dimensional titanium carbide MXenes. *Phys. Chem. Chem. Phys.* **2016**, *18*, 20256−20260.
(16) Tygesen, A. S.; Pandey, M.; Vegge, T.; Thygesen, K. S.; García-Lastra, J. M. Role of long-range dispersion forces in modeling of MXenes as battery electrode materials. *J. Phys. Chem. C* **2019**, *123*, 4064−4071.
(17) Lu, M.; Han, W.; Li, H.; Zhang, W.; Zhang, B. There is plenty of space in the MXene layers: The confinement and fillings. *J. Energy Chem.* **2020**, *48*, 344−363.
(18) Naguib, M.; Kurtoglu, M.; Presser, V.; Lu, J.; Niu, J.; Heon, M.; Hultman, L.; Gogotsi, Y.; Barsoum, M. W. Two-dimensional nanocrystals produced by exfoliation of Ti3AlC2. *Adv. Mater.* **2011**, *23*, 4248−4253.
(19) Tang, Q.; Zhou, Z.; Shen, P. Are MXenes Promising Anode Materials for Li Ion Batteries? Computational Studies on Electronic Properties and Li Storage Capability of Ti_3C_2 and $Ti_3C_2X_2$ (X = F, OH) Monolayer. *J. Am. Chem. Soc.* **2012**, *134*, 16909−16916.
(20) Hu, T.; Hu, M.; Gao, B.; Li, W.; Wang, X. Screening Surface Structure of MXenes by High-Throughput Computation and Vibrational Spectroscopic Confirmation. *J. Phys. Chem. C* **2018**, *122*, 18501−18509.
(21) Khazaei, M.; Arai, M.; Sasaki, T.; Chung, C.-Y.; Venkataramanan, N. S.; Estili, M.; Sakka, Y.; Kawazoe, Y. Novel electronic and magnetic properties of two-dimensional transition metal carbides and nitrides. *Adv. Funct. Mater.* **2013**, *23*, 2185−2192.
(22) Li, T.; Yao, L.; Liu, Q.; Gu, J.; Luo, R.; Li, J.; Yan, X.; Wang, W.; Liu, P.; Chen, B.; Zhang, W.; Abbas, W.; Naz, R.; Zhang, D. Fluorine-Free Synthesis of High-Purity Ti3C2Tx (T = OH, O) via Alkali Treatment. *Angew. Chem., Int. Ed.* **2018**, *57*, 6115−6119.
(23) Bao, Z.; Lu, C.; Cao, X.; Zhang, P.; Yang, L.; Zhang, H.; Sha, D.; He, W.; Zhang, W.; Pan, L.; Sun, Z. Role of MXene surface terminations in electrochemical energy storage: A review. *Chin. Chem. Lett.* **2021**, DOI: 10.1016/j.cclet.2021.02.012.
(24) Persson, P. O. Å.; Rosen, J. Current state of the art on tailoring the MXene composition, structure, and surface chemistry. *Curr. Opin. Solid State Mater. Sci.* **2019**, *23*, 100774.
(25) Persson, I.; Näslund, L.-Å.; Halim, J.; Barsoum, M. W.; Darakchieva, V.; Palisaitis, J.; Rosen, J.; Persson, P. O. Å. On the organization and thermal behavior of functional groups on Ti3C2MXene surfaces in vacuum. *2D Mater.* **2018**, *5*, 015002.
(26) Kresse, G.; Furthmüller, J. Efficient iterative schemes for *ab initio* total-energy calculations using a plane-wave basis set. *Phys. Rev. B: Condens. Matter Mater. Phys.* **1996**, *54*, 11169−11186.
(27) Kresse, G.; Furthmüller, J. Efficiency of *ab-initio* total energy calculations for metals and semiconductors using a plane-wave basis set. *Comput. Mater. Sci.* **1996**, *6*, 15−50.
(28) Kresse, G.; Hafner, J. *Ab initio* molecular-dynamics simulation of the liquid-metalamorphous- semiconductor transition in germanium. *Phys. Rev. B: Condens. Matter Mater. Phys.* **1994**, *49*, 14251−14269.
(29) Csonka, G. I.; Perdew, J. P.; Ruzsinszky, A.; Philipsen, P. H. T.; Lebègue, S.; Paier, J.; Vydrov, O. A.; Ángyán, J. G. Assessing the performance of recent density functionals for bulk solids. *Phys. Rev. B: Condens. Matter Mater. Phys.* **2009**, *79*, 155107.
(30) Kresse, G.; Joubert, D. From ultrasoft pseudopotentials to the projector augmented-wave method. *Phys. Rev. B: Condens. Matter Mater. Phys.* **1999**, *59*, 1758−1775.
(31) Grimme, S.; Antony, J.; Ehrlich, S.; Krieg, H. A consistent and accurate *ab initio* parametrization of density functional dispersion correction (DFT-D) for the 94 elements H-Pu. *J. Chem. Phys.* **2010**, *132*, 154104.
(32) Momma, K.; Izumi, F. VESTA 3 for three-dimensional visualization of crystal, volumetric and morphology data. *J. Appl. Crystallogr.* **2011**, *44*, 1272−1276.
(33) Henkelman, G.; Uberuaga, B. P.; Jónsson, H. A climbing image nudged elastic band method for finding saddle points and minimum energy paths. *J. Chem. Phys.* **2000**, *113*, 9901.